Korean J. Chem. Eng., 39(11), 3003-3011 (2022)
DOI: 10.1007/s11814-022-1210-4

pISSN: 0256-1115
eISSN: 1975-7220

EMI-BF_4 electrolyte and Al_2O_3/PVDF-HFP modified PE separator for high capacitance retention and cycle stability in supercapacitors

Latifatu Mohammed*,†, Bismark Boating*, Manasi Mwemezi, Louis Hamenu***,†, Alfred Madzvamuse****, Alex Nyarko*****, Mutala Mohammed*, William Oduro*, Francis Boateng Agyenim*, Yong Min Lee******, and Jang Myoun Ko****

*Institute of Industrial Research, Council for Scientific and Industrial Research, P. O. Box LG 576, 92 Boundary Road, East Legon, Ghana
**Department of Applied Chemistry & Biotechnology, Hanbat National University, 125 Dongseo-daero, Deokmyeong-dong, Yuseong-gu, Daejeon 34158, Korea
***Department of Chemistry, School of Physical and Mathematical Sciences, College of Basic and Applied Sciences University of Ghana, Legon, Ghana
****Department of Chemistry, University of Zimbabwe, P. O. MP 167, Mount Pleasant, Harare, Zimbabwe
*****Avery Dennison, 171 Draketown road, Pennsylvania, USA, PA 17751
******Department of Energy Science and Engineering, Daegu Gyeongbuk Institute of Science and Technology (DGIST), 333 Techno Jungang-daero, Hyeonpung-eup, Dalseong-gun, Daegu 42988, Korea
(*Received 7 January 2022 • Revised 30 May 2022 • Accepted 16 June 2022*)

Abstract−Polyolefin separators are inherently hydrophobic and thermally unstable, contributing to poor cycle performance and high thermal shrinkage, respectively, which can shorten cycle life. Herein, a high-performance supercapacitor based on a composite separator made from nano-Al_2O_3/PVDF-coated on polyethylene (PE) polyolefin substrate was prepared using a low-cost casting (stir-dip-coat-dry) technique and an electrolyte containing 1 M EMI-BF_4 salt in EC : EMC : DMC (1 : 1 : 2 vol%) is reported. The results show that integration of nano-Al_2O_3 in the PVDF matrix contributes to a large interactive surface area that attenuates interfacial energy at the separator-electrolyte boundary and improves porosity as well as the overall performance. The filler also enhances high mechanical anchoring onto the PE substrate, contributing to the overall physical and electrochemical properties of the separator. These modified PE separators with porous microstructure demonstrate superior electrolyte wettability (88%), stable electrochemical performance, and high cycle stability superior to analogous cells with commercial separators. The pair of coated modified separators with the 1 M EMI-BF_4 modified electrolyte registered a high ionic conductivity value of 2.23 mS/cm. This facile technique is scalable for separator-electrolyte design and is attractive for low-cost supercapacitor manufacturing which is safe and fast charging.

Keywords: Supercapacitor, Surface-modified Separator, Large Interactive Surface Area, Ionic Electrolyte, Lower Interfacial Energy

INTRODUCTION

Over the past few decades, key players in the energy community have unequivocally raised concerns about the fast depletion of fossil fuels and the need to find a suitable replacement that wields the requisite potential for high-energy and ultra-high power density systems comparable to fossil fuels [1-3]. Among the suitable energy storage systems available, the electrochemical supercapacitor stands out, owing to its high energy per unit volume, rapid charge/discharge, and ultra-high number of cycles [4]. Supercapacitors have found widespread application in a host of electrical and electronic systems, including electric vehicles, buses, trains, cranes, and elevators [5]. However, the theoretical expectations of supercapacitors are far ahead of the achieved specific capacitance in real-life applications owing to many factors, including issues relating to the electrode material properties [6,7], electrolyte composition [8,9], and the characteristics of the membrane separator [10]. Amongst these three major components of the supercapacitor mentioned, the membrane separator is the least investigated because it is an inactive component in a typical supercapacitor setup. Meanwhile, the membrane separator plays a critical role in ensuring the safety and smooth running of the supercapacitor. It electrically isolates the anode from the cathode, ensuring the efficient shuttling of ions, blocking of active solid materials, and serving as an electrolyte reservoir, which ensures effective supply of ions during the charge/discharge process [11-13]. Achieving these benchmarks in a typical membrane separator is key to ensuring the smooth and efficient cycling of supercapacitors.

Polyolefin separators used in the lithium-ion battery (LIB) possess excellent chemical stability, superior mechanical properties and are relatively inexpensive. It remains the most used commercial LIB

†To whom correspondence should be addressed.
E-mail: latifatu.mohammed@yahoo.com, imohammed@gmail.com, lhamenu@ug.edu.gh

Table 1. Physical constants of organic carbonate solvents used in this study [36]

Solvent	Molar volume (25 °C) $dm^3\ mol^{-1}$	Dipole moment (l/D)	Dielectric constant (25 °C)	Melting temperature (°C)
Ethylene carbonate (EC)	62	4.9	89	37
Ethylene methyl carbonate (EMC)	104	-	2.9	−55
Dimethyl carbonate (DC)	84	0.88	3.12	3

separator despite intense research which has focused on the use of cellulose composite membranes, polyvinylidene fluoride, and other materials in the fabrication of LIB in recent years. Its demerits lie in the aged problem of poor electrolyte wettability, uptake and retention of the same, leading to its poor ionic conductivity. Separator engineering through surface modifications, multi-layering designs, and particulate doping has helped to incorporate essential properties into the separator to enhance its performance with each technique introducing its own challenges and merits [14-21]. Some surface modification techniques have found commercial usage [22-24]. The existing modification approaches reported in literature for polyolefin separators involve a complex combination of time, sophisticated equipment, and chemical processes before arriving at the desired material texture and monodispersity, making it ineffective for industrial application [25-32]. Furthermore, most of the modified separators have gained more applications in lithium-ion batteries with very little to do with supercapacitors. The application and study of polyolefin separators in supercapacitors is very important in finding alternative improved separators that will offer excellent supercapacitor properties.

This study reports the dual process of achieving better capacitance and cycle life stability using a combination of membrane separator surface modification and electrolyte engineering through a facile, cost-effective, and scalable separator surface modification approach that could be utilized at an industrial level with ease in supercapacitors. The surface modification approach is realized by directly submerging the commercial separator into Al_2O_3/PVDF (both commercially sourced) solution and simply drying it in an oven. The introduction of aluminum oxide particles into the PVDF matrix imparts strong anchoring to the polymer chains and to the membrane substrate, which mitigates delamination on the coated separator. Moreover, the incorporation of the closely packed nano-Al_2O_3 introduces unique coating characteristics comprising a well-connected and homogeneous nanoporous structure that can be filled with the liquid electrolyte, hence providing a facile pathway for fast ion movement. The electrolyte engineering approach is also achieved by simply dissolving 1 M 1-ethyl-3-methylimidazolium tetrafluoroborate (EMI-BF_4) salt in EC : EMC : DMC (1 : 1 : 2 vol%). The choice of EMI-BF_4, ionic liquid is due to its wider electrochemical stability window and comparatively good ionic conductivity with other ionic liquids [33,34]. The electrochemical properties of supercapacitors employing the modified separators were investigated using a ternary solvent system: EC : EMC : DMC (1 : 1 : 2 vol%) instead of the traditional solvent, acetonitrile, which cannot be used in supercapacitors for consumer applications, such as toys, electric backup systems, and electric vehicles [35]. The solvents have different dielectric permittivity, melting temperatures, different viscosity values, and dipole moments (See Table 1). The solubility of salts in these solvents is also different [36].

EXPERIMENTAL PROCEDURE

1. Materials and Chemicals

All the materials for this study were commercially sourced. 1-ethyl-3-methylimidazolium tetrafluoroborate (EMIBF_4), ethylene carbonate (EC) ethyl methyl carbonate (EMC) dimethyl carbonate (DMC), acetone, poly(vinylidene fluoride (PVDF), and N-methyl pyrrolidone (NMP) of the highest purity were obtained from Sigma Aldrich and used without further treatment. The nano-Al_2O_3 particle with an average size of 13 nm (Aerosil-Alu C, surface area ($100\pm15\ m^2g^{-1}$)). The vapor-grown carbon fiber (VGCF) and activated carbon (MSC-30) were obtained from Kansei Coke, Japan. The activated carbon used has a BET surface area of 3,125 m^2/g, BJH surface of 1,787 m^2/g, an average pore diameter of 2.312 nm, and a total pore volume of 1.033 cm^3/g. Poly(vinylidene fluoride-co-hexafluoropropylene) (PVdF-HFP) powder was sourced from Kynar Flex®2801, Arkema Inc., and aluminum oxide (Al_2O_3) powder was purchased from AES-11, Sumitomo Chemical Co. A Commercially available polyolefin separator (Monolayer PE, 20 μm thick, porosity 45%) was employed as substrate for the experiment. All materials were used as received without further purification.

2. Activated Carbon Electrode Preparation

Typically, Al foil washed with distilled water and acetone for 30 min in a sonicator was dried in an oven at 70 °C for 6 hours. The dried Al foil was then cut into 1 cm×4 cm size to be employed as the current collector. Activated carbon and VGCF in 8 : 1 ratio were mixed in a mortar until a uniform mixture was obtained. Then 1 part of 10 wt% PVDF/NMP binder solution was added to the mixture and further mixed to form a homogeneous slurry. Some of this slurry was pipetted and coated onto a 1 cm×1 cm area of the current collector. The electrode was dried in a vacuum oven at 80 °C for 24 hours to ensure even drying. The final electrode comprising activated carbon, PVDF binder, and VGCF in the ratio of 8 : 1 : 1 was used as the conductive agent.

3. Preparation of Electrolyte Solution and Surface-modified PE Separator

The electrolyte solution was prepared in a glove box, with 1 M EMIBF_4 salt dissolved in EC : EMC : DMC 1 : 1 : 2 (by volume) and stirred to obtain uniformity. The electrolyte solution was allowed to stay undisturbed for 6 hours to ensure complete dissolution. The as-synthesized solution was utilized in the fabrication of the cells. A 0.1 g mass of PVDF-HFP was dissolved in 8.0 g of acetone at 45 °C. A 0.1 g Al_2O_3 was added to the PVDF-HFP suspension and stirred for 6 hours at room temperature to the dissolved PVDF-

HFP to obtain a uniform mixture. A predefined size of PE separator was dipped into the Al_2O_3/PVDF-HFP blend to cover both sides of the separator. The dip-coated separators were air-dried for 30 minutes and oven dried for 6 hours at 60 °C to obtain an Al_2O_3/PVDF-HFP-PE-Al_2O_3/PVDF-HFP composite structure which was used for cell assembly. The uncoated PE separator was employed as a control.

4. Characterization of Modified Separator

The as-fabricated separator and the electrolyte properties were characterized to evaluate their respective performance. The coated separator surface was examined using field-emission scanning electron microscopy (FE-SEM, S4800, Hitachi, Japan) to examine the topological morphology. The wettability of the separator was evaluated using contact angle analyzers (Surface Electro-Optics Co., Ltd., South Korea) recorded at t=2 s to assess the separator-electrolyte interfacial resistance.

Linear sweep voltammetry tests were run within the potential range of 0-5.0 V at a scan rate of 10 mV/s employing nickel electrodes separated by the PE coated separator and the electrolyte using an Autolab PGstat 100, Eco Chemie potentiostat/galvanostat instrument to evaluate electrochemical stability of both the modified separator and the as-synthesized electrolyte. Finally, the bulk conductivities of the coated separators filled with the electrolyte were determined against platinum electrodes using the Autolab PARSTAT 12/30 potentiostat/galvanostat. A frequency response analyzer within a frequency range of 0.01 Hz to 1 MHz was used to evaluate the ionic conductivity when the cell was assembled. The resistivity (ρ) in Ωcm^{-1} of the separators in 1 M $EMIBF_4$ (EC : EMC : DMC) was estimated according to Eq. (1):

$$\rho = \left(\frac{d}{R_s \times S}\right) \tag{1}$$

where R_s is the solution resistance obtained from the Nyquist plot real axis in the high-frequency region; d, the thickness of the separator between the two electrodes; S is the area of the electrodes.

The electrochemical stability window of the different separators was determined using linear sweep voltammetry (LSV). The half-cell consisted of stainless steel as the working electrode with lithium metal as the counter and the reference electrode in a potential range of 0 V-5.0 V using a scan rate of 1.0 mV/s.

5. Supercapacitor Fabrication and Testing

Full cells were constructed by placing a 2×2 cm^2 coated separator between two AC electrodes, which were assembled and sealed within an aluminum pouch. Complete cell assembly was done with the modified and pristine separators and with the 1 M $EMIBF_4$ (EC : EMC : DMC) electrolyte injection in an argon-filled glove box. To conduct the cyclic voltammetry (CV) test, the oxidation cutoff potentials for the cyclic voltammetry tests were fixed at 3.0 V and 3.5 V, while the reduction cutoff potential stayed fixed at 0 V. Cyclic voltammograms were measured at scan rates of 20 mV/s, 50 mV/s, 100 mV/s, 200 mV/s, 300 mV/s, and 500 mV/s. The specific capacitance (C) was calculated as a function of scan rate using Eq. (2) below:

$$C = \frac{|qa + qc|}{(2m\Delta V)} \tag{2}$$

where qa, qc, m, and ΔV denote anodic, cathodic charges, the mass of the active material, and the potential window of the cyclic voltammetry scan, respectively. The resistive components of the full cells were investigated directly after the CV test using the electrochemical impedance spectroscopy technique. An Autolab PARSTAT 12/30 potentiostat/galvanostat, frequency response analyzer was used for this analysis in a frequency range of 10 mHz-1 MHz. Cycling tests were conducted at a 200 mV/s scan rate and a potential range of 0 V-3.0 V and 0 V-3.5 V over 500 cycles. Galvanostatic charge-discharge was also performed at a current density of 5 mA/cm^2 over the potential ranges of 0-3.0 V and 0-3.5 V.

The functionality of the symmetric supercapacitors is better defined by the power density (Pd) and the energy density (Ed) factors. The energy density and the power density of the cells at the different voltages were estimated from the charge-discharge data using the equations below:

$$Cs = \frac{I\Delta t}{mV} \tag{3}$$

$$Ed = \frac{CsV^2}{2} \tag{4}$$

$$Pd = \frac{Ed}{\Delta t} \tag{5}$$

where Cs, I, m, V, and Δt represent the specific discharge capacitance, applied current, combined mass of loading, cell voltage, and the discharge time after ohmic drop.

RESULTS AND DISCUSSION

1. Characterization of Modified Separator

The morphological characterization of the pristine PE and modified PE separators is depicted in Fig. 1. The topological evaluation of the conventional PE separator reveals a microporous structure typical of commercial separators [Fig. 1(a)]. On the other hand, the modified separator topology shows nanoporous and pinhole structures [Fig. 1(b)] interspersed with anchored nano-Al_2O_3 particles within the PVDF matrix. The nano-porous and pinhole structures of the modified separator create a high surface area, which is vital for attenuating the solid-liquid interfacial energy. Moreso, the presence of the widely dispersed and anchored nano-Al_2O_3 particles in the polymer matrix enhances the strong physical bonding of the polymer chains [37], thus influencing the overall performance of the separator during operation. The availability of the filler material in the polymer matrix thus reduces the surface energy that can influence wettability. To evaluate the wettability of the separator, the contact angle test (Fig. 2) was performed at the early electrolyte-separator contact (t=2 s), which is done to assess the solid-liquid interfacial energy of the various separators. The results revealed that coating Al_2O_3/PVDF layer on the PE significantly attenuated the interfacial energy of the Al_2O_3/PVDF/PE composite separator (~10.92°), making the surface more hydrophilic compared to the pristine PE separator (43.14°). This translated into the increase in wettability, uptake, and retention of electrolytes in the composite separator, which are critical parameters for ensuring the steady supply of ions needed to stabilize the running of the super-

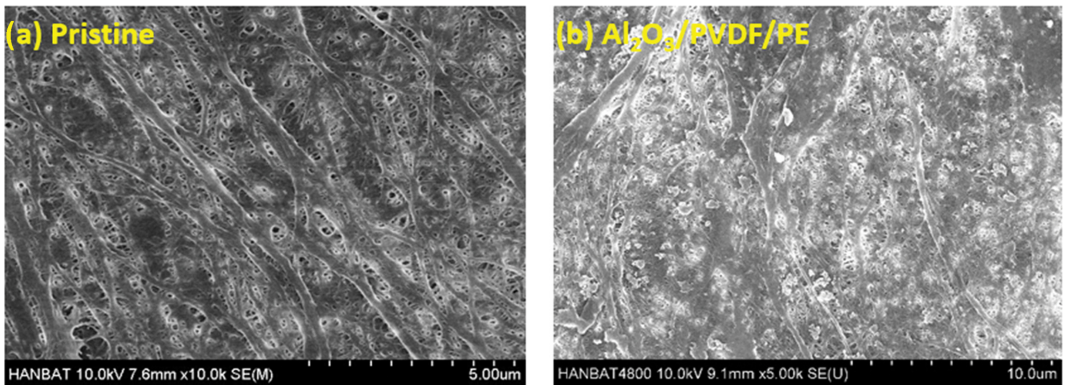

Fig. 1. Force emission scanning electron microscope images of (a) pristine separator, (b) Al_2O_3/PVDF/PE separator.

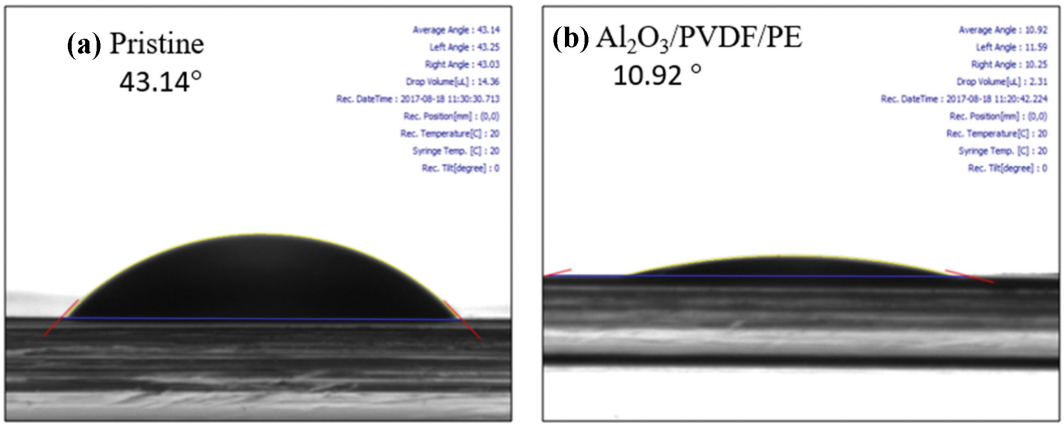

Fig. 2. Contact angle pictures of (a) Pristine separator, (b) Al_2O_3/PVDF/PE separator.

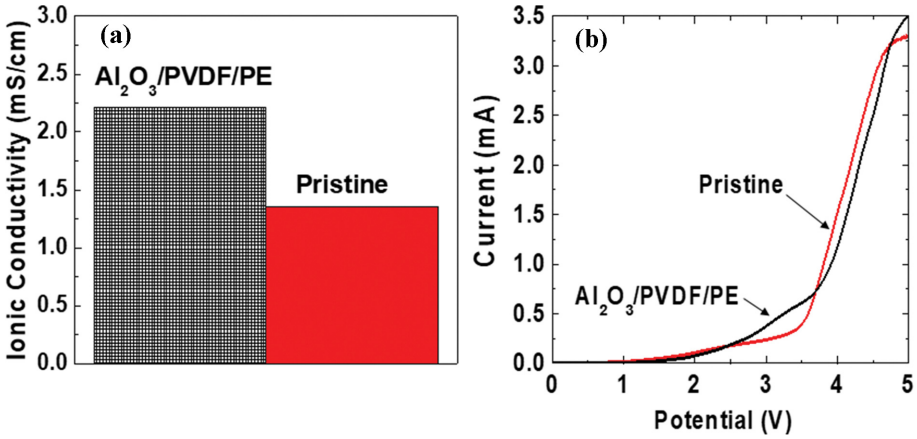

Fig. 3. (a) Ionic conductivity values of the Al_2O_3/PVDF/PE and the pristine separator, (b) Linear sweep voltammogram of the coated separator and the uncoated separator.

capacitor.

A commercial PE separator was utilized as substrate due to its inherently excellent mechanical properties and electrochemical stability, and therefore coating the PE separator with thermally stable, highly amorphous, and hydrophilic layer improves its thermal stability, electrolyte wettability, uptake, and retention [38,39]. Thus, coating the pristine PE with the Al_2O_3/PVDF improves cell safety while enhancing ionic transport and stable cycle performance. Fig. 3(a) shows the ionic conductivity of the Al_2O_3/PVDF/PE separators and pristine separators in the 1 M $EMIBF_4$ (EC : EMC : DMC) electrolyte. The Al_2O_3/PVDF/PE separator has a slightly higher ionic conductivity in the electrolyte compared to the pristine electrolyte. This is ascribed to the presence of the hydrophilic layer on the PE substrate with enhanced ionic pathways, thus increasing the electrolyte uptake of the modified separator and improving ionic conductivity. The performance of the as-modified separator

Table 2. Summary of polyolefin separators modified ceramic particles

Polyolefin substrate	Ceramic particles (size)	Reagents	Binding material	Technique and equipment	Thickness (Pristine/ modified separators (μm)	Electrolyte	Ionic conductivity (mS/cm)	Oxidation potential (Li/Li^+)	Electrolyte uptake (%)	Contact angle (°)	Reference
PE	Al_2O_3 (1.5 μm)	Ammonium acrylate, silicone surfactant, CMC, Water	Polyacrylate	Planetary ball milling, spreader coating process	20/26	1 M $LiPF_6$ in EC : DEC : DMC	0.75	4	144	11.6	19
PE	Boehmite (AlOOH-1.4 μm)	Ammonium acrylate, silicone surfactant, CMC, Water	Polyacrylate	Planetary ball milling, spreader coating process	20/26	(1 M $LiPF_6$ in EC : DEC : DMC	1.0	5	187	5.7	19
PE	Boehmite-AlOOH (350 nm)	Water	PVA	Grinding machine, Roller coating instrument	16/17.15	$LiPF_6$ in EC : DEC	6.56			Nearly zero	20
PP-PE-PP	Zirconium dioxide	Ethanol, TAH, DHC, 1-PrOH, Zr(O-n-Pr)4	Dopamine	Sol-gel process	25.01/25.33	1.2 M $LiPF_6$ in EC/DMC/ DEC	3.469	4.08	186	30.4	21
PE	SiO_2 (50 and 100 nm)	MPTS, BTO, AIBN, MeOH, toluene	No binder	UVO, Chemical grafting	15/500	1 M $LiPF_6$ in EC/EMC	0.82			84	22
PE	Al_2O_3 (430 nm)	DHC, MeOH	CMC	Polydopamine treatment method	20/27	1 M $LiPF_6$ in EC/EMC	0.79		119.0	63	23
PP	Al_2O_3 (200-300 nm), SiO_2 (50 nm)	DMAC, and Propylene glycol monomethyl ether acetate	PVDF-HFP	Solution casting	20/22	1 M $LiPF_6$ in EC/DEC	0.78		125		24
PE	Nano-CeO (5 and 10 μm)	DMF	P(MMA-BA-AN-St)	Solution casting	18/75.3	1 M $LiPF_6$ EMC/EC/ DEC	2.5	5	79		25
PE	Al_2O_3 (430 nm)	DI water	CMC	Plasma treatment and solution casting	20/26	$LiPF_6$ EC/EMC	1.182	4.3	85	70	26
PE	**Al_2O_3 (13 nm)**	**Acetone**	**PVDF**	**Dip-coating**	**20/25**	**1 M $EMIBF_4$ (EC : EMC : DMC)**	**2.23**	**5**	**89**	**10.75**	**This work**

was compared with most related findings in the literature and the results are summarized in Table 2. The evidence shows that the Al_2O_3/PVDF-modified PE separator improves the most essential properties of a separator required for electrochemical cell performance and stability.

The electrochemical compatibility of the modified separator and the electrolyte was also evaluated using linear sweep voltammetry (LSV) characterization to assess the stability of the cells containing the modified separator and electrolyte within the electrochemical window. As shown in Fig. 3(b), the LSV curve of the cell sweeps from 0.0 V to 5.0 V at a constant rate of 10 mV/s, which demonstrates anodic electrochemical compatibility and stability within the cell. Thus typifying the wide electrochemical window of the modified electrolyte during cycling and for the oxidation of BF_4^- ions [40]. From the micrograph, the onset of oxidation for the modified separators starts slightly early compared to the pristine separator. This may be attributed to traces of water on the modified separator.

2. Supercapacitor Performance

The electrochemical performance of the cells employing the pristine PE and modified PE separators in the 1 M $EMIBF_4$ (EC : EMC :

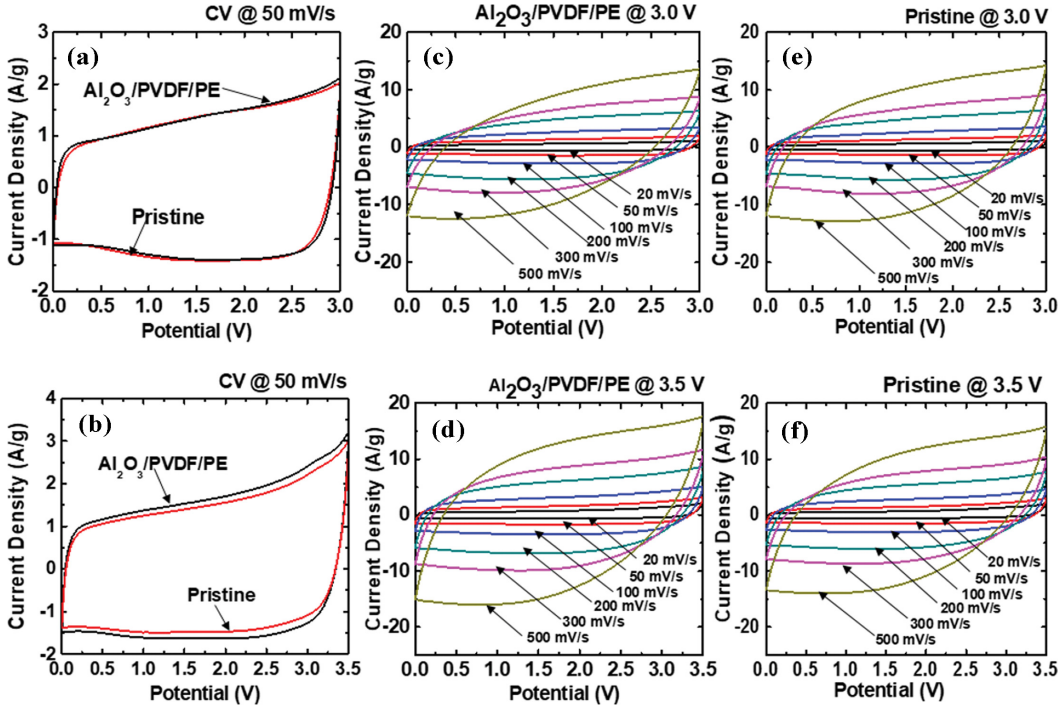

Fig. 4. Cyclic voltammograms of supercapacitors with (a) Al_2O_3/PVDF/PE and the pristine separators at a potential range of 0-3.0 V, (b) Al_2O_3/PVDF/PE and the pristine separators at a potential range of 0-3.5 V, (c) Al_2O_3/PVDF/PE separator at a potential range of 0-3.0 V, (d) Al_2O_3/PVDF/PE separator at a potential range of 0-3.5 V, (e) Pristine separator at a potential range of 0-3.0 V, (f) Pristine separator at a potential range of 0-3.5 V; at different scan rate.

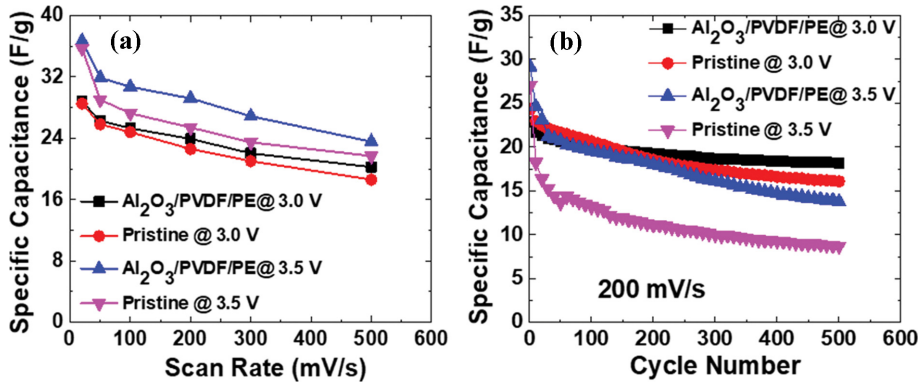

Fig. 5. Specific capacitance of the supercapacitor with the Al_2O_3/PVDF/PE and pristine separators at different potentials (a) as a function of scan rate, (b) as a function of cycle number.

DMC) electrolytes was evaluated at different potentials (0 V-3 V and 0 V-3.5 V and at different rates. As shown in Fig. 4, the CV curves for the pristine PE and modified PE separators show a rectangular shape, which is typical of an electric double layer; and this indicates that the charge storage occurs at the electrode/electrolyte interphase [41,42]. A distortion in the rectangular shape is observed at a higher potential for all the samples. Comparing the CVs of the various cells at the different potentials, it can be observed that the size of the voltammograms of the supercapacitors made of the modified PE separators at both voltages is higher than those employing the pristine PE at all scan rates. This can be ascribed to the increased ionic conductivity (See Fig. 3(a)) and better electrolyte uptake of the modified separator (See Fig. 2). At increasing scan rate, the shape of the voltammograms of the supercapacitors employing the different separators shifted from the normal rectangular shape with lower current density response (see Fig. 4(c), (d), (e), and (f)), which indicates that the electrochemical process occurring at a higher scan rate is slightly restricted by the fast movement of ions.

The measured specific capacitances as a function of scan rate of the cells employing the pristine PE and modified PE at 0-3.0 V and 0-3.5 V are shown in Fig. 5(a). The as-fabricated cells at the different potential windows demonstrate decreasing specific capacitance with increasing scan rate. The supercapacitors with the two

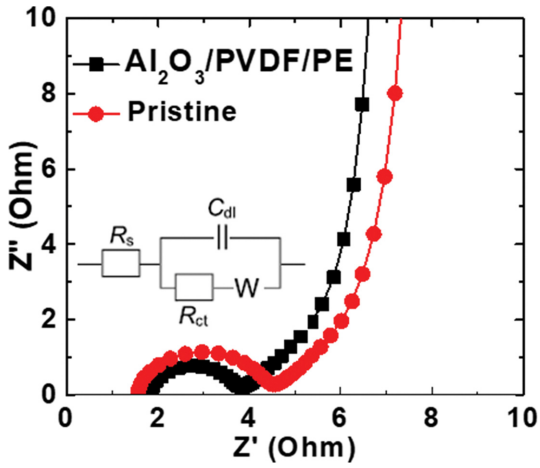

Fig. 6. Nyquist plots of supercapacitors with Al_2O_3/PVDF/PE and pristine separators taken after cyclic voltammetry reading.

separators employing higher potential (0-3.5 V) demonstrate faster decreasing specific capacitance with increasing scan rate compared to the separators at lower potential (0-3.0 V). This behavior can be attributed to the inherent low ionic conductivity of organic electrolytes due to the high viscosity of the organic solvent and their fast oxidation at higher potential [43,44]. The specific capacitances obtained for the different separators at lower potentials are very close over the entire scan rate range (See Fig. 5(a)).

Furthermore, the supercapacitor comprising the modified PE separators maintained higher specific capacitance over the entire scan rate range at both 0 V-3.0 V and 0 V-3.5 V compared to the supercapacitor with the pristine PE separator (See Fig. 5(a)). These interesting results can be ascribed to the excellent compatibility and wettability between the 1 M $EMIBF_4$ (EC : EMC : DMC) and the modified PE separators as demonstrated by the contact angle test and electrolyte uptake test.

The separator-electrolyte interfacial resistance was assessed to evaluate the ion shuttling impedance using the Nyquist analysis. The Nyquist plot of the supercapacitors adopting both separators in 1 M $EMIBF_4$ (EC : EMC : DMC) is depicted in Fig. 6. Table 1 shows the data from Randle equivalent circuit in the inset in Fig. 6. A typical Randle model is made up of bulk resistance (R_s) in the high-frequency region, a charge transfer resistance (R_{ct}, semi-circle), and a block parallel, containing a double layer capacitance (C_d) in the medium frequency region. Included next to the R_{ct} is Warburg impedance (W, showing a sloping straight line) in the low-frequency region [45]. Comparing the two plots, the modified PE separators demonstrate less resistance compared to the supercapacitor with the pristine PE separator. According to Table 3, the supercapacitor with the modified PE separator involves higher R_s (resistance emanating from the electrolyte and the separator) but a lower R_{ct} (the diameter of the semi-circle), whereas the supercapacitor with the pristine PE separator demonstrates lower R_s, but higher R_{ct}. This superior electrochemical observation is ascribed to superior wettability and compatibility between the highly hydrophilic inorganic alumina nanoparticles on the surface of the PE separator and the 1 M $EMIBF_4$ (EC : EMC : DMC) electrolyte. The superior wettability and compatibility contribute to the dual effects of the closely packed nano-Al_2O_3/PVDF hydrophilic layer on the separator and the increased ionic activity in the electrolyte due to the presence of EMI^+ and BF_4^- ionic species.

A cycle test was conducted to evaluate the stability of the separators in the 1 M $EMIBF_4$ (EC : EMC : DMC) electrolytes and within the applied potential windows. The cyclic voltammograms were investigated at 200 mV/s for 500 cycles at different potentials (0 V-3 V and 0 V-3.5 V). The specific capacitance as a function of cycle number is depicted in Fig. 5(b) for the different separators. All cells show a decreasing specific capacitance with increasing cycle number. Notably, the cells with the modified PE separators separator demonstrate superior stability with high specific capacitance compared to the pristine separator at the different potential windows. After 500 cycles, the supercapacitors with the pristine PE separators retained 66.15% and 32.12% of their initial capacitance at 3.0 V and 3.5 V voltage ranges. Comparatively, the modified PE separator retained approximately 79.4% and 47.28% of initial capacitance, respectively, at 3.0 V and 3.5 V voltage ranges. The superior performance of the composite PE membrane can be ascribed to the excellent electrochemical compatibility, adequate pore structure, and better ionic conductivity due to the attenuated separator-electrolyte interfacial energy between the as-fabricated surface of Al_2O_3/PVDF/PE separator and the 1 M $EMIBF_4$ (EC : EMC : DMC) electrolyte system [46]. Fig. 7 shows the galvanostatic charge-discharge results at 5.0 mA/cm^2 and the Ragone plot at 3.0 V and 3.5 V for both separators. The linear shape demonstrated by the charge and discharge of the cells reflects electric double layer capacitor behavior (See Fig. 7(a)). All the cells with the different separators show small ohmic drops at higher voltages. The Al_2O_3/PVDF/PE separator system has a longer charge-discharge cycle time at the two different potential ranges of 0 V-3 V and 0 V-3.5 V in the 1 M $EMIBF_4$ (EC : EMC : DMC) electrolyte compared to the pristine separator. Given that the measurements were recorded at a constant current of 5 mA/cm^2, a longer time of cycle translates to a larger magnitude of energy stored [8]. The modified separator in combination with the electrolyte improves charge storage properties of the supercapacitor and therefore higher capacitance.

The Ragone plot in Fig. 7(b) summarizes the energy and power density calculated for the supercapacitors prepared with the pris-

Table 3. Thickness, electrolyte uptake of Al_2O_3/PVDF/PE separator, and the resistance properties of supercapacitor adapting the Al_2O_3/PVDF/PE separator

Separator	Thickness (μm)	Electrolyte uptake	Solution resistance (R_s)	Charge transfer resistance (R_{ct})
Pristine separator	20	83	1.576	2.792
Al_2O_3/PVDF/PE separator	27	89	1.845	1.926

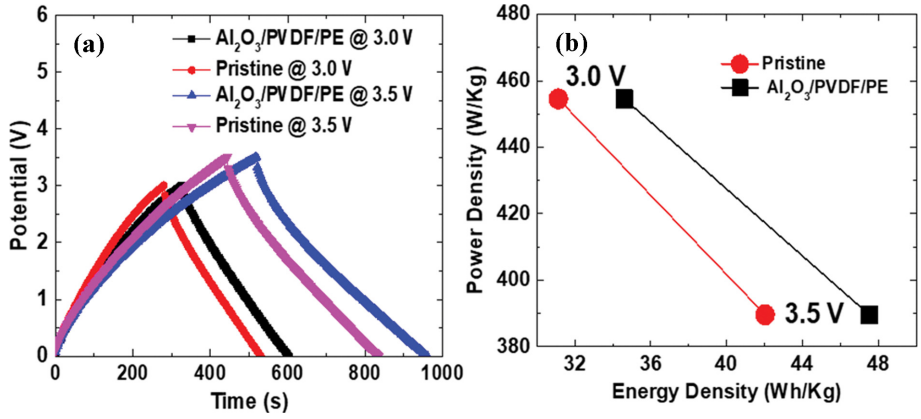

Fig. 7. (a) Galvanostatic charge-discharge (b) the Ragone plots; of the supercapacitor with the Al_2O_3/PVDF/PE and pristine separators at different potential ranges and at a current density of 5 mA/cm^2.

tine separator and the composite separator. At a higher voltage of 3.5 V the energy density of both supercapacitors increased while the power density decreased. This is consistent with the general trend observed for EDLC supercapacitors. At both voltages the supercapacitors made with the composite PE separator had higher energy density (35 WH/kg and 48 WH/kg at 3 V and 3.5 V, respectively) than the pristine PE separator (31 WH/kg and 42 WH/kg at 3 V and 3.5 V, respectively). The power density was the same at each voltage, 455 W/kg at 3 V and 390 W/kg at 3.5 V for both separators. In the composite PE separator supercapacitor, the increase in energy density is balanced by an increase in the rate of discharge of the energy due to the high electrolyte retention ability and ion mobility of the electrolyte species through the separator. The improvement in ionic conductivity of the PE composite separator supercapacitor translated into a higher discharge time but comparable power density with the pristine separator supercapacitors.

CONCLUSION

Supercapacitors were fabricated with nano-Al_2O_3/PVDF modified PE separator and pristine PE separator and their electrochemical properties were investigated in a 1 M $EMIBF_4$ (EC : EMC : DMC) electrolyte system. The results reveal that supercapacitor configuration comprised of nano-Al_2O_3/PVDF modified separator and 1 M $EMIBF_4$ (EC : EMC : DMC) electrolyte achieves a highly stable electrochemical and cycle performances. The observed stability of the composite PE separator system is attributed to the presence of hydrophilic structure on the separator that leads to attenuated separator-electrolyte interfacial resistance and the increased ionic activity in the electrolyte due to the presence of EMI^+ and BF_4^- ionic species. This engineered separator and electrolyte is a simple, scalable, and effective route to achieving electrochemical superiority and industrial replicability.

ACKNOWLEDGEMENT

The research team would like to acknowledge the applied electrochemistry laboratory at Hanbat National University, South Korea for supporting this work.

LIST OF ABBREVIATION

DMF	: N, N-dimethylformamide
PVDF	: polyvinylidene fluoride
Al_2O_3	: aluminum oxide
CMC	: sodium carboxymethyl cellulose
P(MMA-BA-AN-St)	: PVDF-HFP-polyvinylidene fluoride-hexafluoropropylene
PVA	: polyvinyl alcohol
AlOOH	: boehmite
MeOH	: methanol
DHC	: dopamine hydrochloride
DMAC	: dimethylacetamide
SiO_2	: silicon dioxide
EC	: ethylene carbonate
DEC	: diethylene carbonate
$LiPF_6$	: lithium hexafluorophosphate
DMC	: dimethyl carbonate
DEC	: diethyl carbonate
$ZrO\text{-}n\text{-}Pr)_4$	: zirconium propoxide solution
$EMIBF_4$	: 1-ethyl-3-methylimidazolium tetrafluoroborate
TAH	: tris(hydroxymethyl)aminomethane hydrochloride
AIBN	: azobisisobutyronitrile
UVO	: ultraviolet ozone
MPTS	: 3-methacryloxypropyltrimethoxysilane
BTO-1,8	: bis(triethoxysilyl)
PrOH	: propanol
Nano-CeO_2	: nano cerium oxide

REFERENCES

1. Q. Li, J. Chen, L. Fan, X. Kong and Y. Lu, *Green Energy Environ.*, **1**, 18 (2016).
2. C. Weng, J. Sun and H. Peng, *J. Power Sources*, **258**, 228 (2014).
3. R. Hausbrand, G. Cherkashinin, H. Ehrenberg, M. Gröting, K. Albe, C. Hess and W. Jaegermann, *Mater. Sci. Eng. B*, **192**, 3 (2015).
4. M. Hwang and J. S. Jeong, *Korean J. Chem. Eng.*, **38**, 454 (2021).
5. H. Yu, Q. Tang, J. Wu, Y. Lin, L. Fan, M. Huang, J. Lin, Y. Li and F. Yu, *J. Power Sources*, **206**, 463 (2012).

6. M. Latifatu, J. H. Park, J. M. Ko and J. Park, *J. Ind. Eng. Chem.*, **63**, 12 (2018).
7. L. Mohammed, H. Mengyang, H. Louis, A. Madzvamuse, A. Nyamful, D. Dodoo-Arhin, A. Danquah, O. K. Manteaw, M. N. Zainudeen, S. A. Darkwa, J. H. Park and J. M. Ko, *Int. J. Electrochem. Sci.*, **16**, 210756 (2021).
8. L. Hamenu, A. Madzvamuse, M. Hu, L. Mohammed, C. Y. Bon, S. J. Kim, W. I. Cho, J. Park and J. M. Ko, *Curr. Appl. Phys.*, **17**, 1639 (2017).
9. A. Madzvamuse, L. Hamenu, L. Mohammed, C. Y. Bon, S. J. Kim, J. H. Park and J. M. Ko, *J. Electrochem. Sci. Technol.*, **8**(4), 314 (2017).
10. K. M. Kim, M. Latifatu, Y.-G. Lee, J. M. Ko, J. H. Kim and W. I. Cho, *J. Electroceram.*, **32**, 146 (2014).
11. G. Li, C. Wang, W. Cai, Z. Lin, Z. Li and S. Zhang, *NPG Asia Mater.*, **8**(10), 317 (2016).
12. Z. Wei, Y. Ren, J. Sokolowski, X. Zhu and G. Wu, *InfoMat*, **2**(3) 483 (2020).
13. H. Lee, M. Yanilmaz, O. Toprakci, K. Fu and X. Zhang, *Energy Environ. Sci.*, **7**(12), 3857 (2014).
14. B. Boateng, X. Zhang, C. Zhen, D. Chen, Y. Han, C. Feng, N. Chen and W. He, *Nano Sel.*, **2**(6) 993 (2021).
15. B. Boateng, Y. Han, C. Zhen, G. Zeng, N. Chen, D. Chen, C. Feng, J. Han, J. Xiong, X. Duan and W. He, *Nano Lett.*, **20**(4), 2594 (2020).
16. J. Zhao, D. Chen, B. Boateng, G. Zeng, Y. Han, C. Zhen, J. B. Goodenough and W. He, *J. Power Sources*, **451**, 227773 (2020).
17. X. Shi, Q. Sun, B. Boateng, Y. Niu, Y. Han, W. Lv and W. He, *J. Power Sources*, **414**, 225 (2019).
18. B. Boateng, G. Zhu, W. Lv, D. Chen, C. Feng, M. Waqas, S. Ali, K. Wen and W. He, *Phys. Status Solidi - Rapid Res. Lett.*, **12**(10), 1800319 (2018).
19. Y. Wang, Q. Wang, Y. Lan, Z. Song, J. Luo, X. Wei, F. Sun, Z. Yue, C. Yin, L. Zhou and X. Li, *Solid State Ion.*, **345**, 115188 (2020).
20. C. Yang, H. Tong, C. Luo, S. Yuan, G. Chen and Y. Yang, *J. Power Sources*, **348**, 80 (2017).
21. L. Liu, Y. Wang, C. Gao, C. Yang, K. Wang, H. Li and H. Gu, *J. Membr. Sci.*, **592**, 117368 (2019).
22. W. Na, K. H. Koh, A. S. Lee, S. Cho, B. Ok, S. W. Hwang, J. H. Lee and C. M. Koo, *J. Mater. Sci.*, **573**, 621 (2019).
23. H. Lee, H. Jeon, S. Gong, M. H. Ryou and Y. M. Lee, *Appl. Surf. Sci.*, **427**, 139 (2018).
24. H. Liu, J. Xu, B. Guo and X. He, *Ceram. Int.*, **40**(9), 14105 (2014).
25. X. Luo, Y. Liao, Y. Zhu, M. Li, F. Chen, Q. Huang and W. Li, *J. Power Sources*, **348**, 229 (2017).
26. H. Jeon, S. Y. Jin, W. H. Park, H. Lee, H. T. Kim, M. H. Ryou and Y. M. Lee, *Electrochim. Acta*, **212**, 649 (2016).
27. J. Mun, T. Yim, Y. G. Kwon and K. J. Kim, *Chem. Eng. J.*, **405**, 125844 (2021).
28. V.-C. Ho, B. T. D. Nguyen, H. Y. N. Thi, J. F. Kim and J. Mun, *Int. J. Energy Res.*, **46**(4), 5177 (2021).
29. P. J. Kim, *Nanomaterial*, **11**, 2275 (2021).
30. H. Lee, M. Yanilmaz, O. Toprakci, K. Fu and X. Zhang, *Energ. Environ. Sci.*, **7**, 3857 (2014).
31. J. R. Rodriguez, P. J. Kim, K. Kim, Z. Qi, H. Wang and V. G. Pol, *J. Colloid Interface Sci.*, **583**, 362 (2021).
32. Q. N. Tran, I. T. Kim, J. Hur, J. H. Kim, H. W. Choi and S. J. Park, *Korean J. Chem. Eng.*, **37**(5). 898 (2020).
33. S. Pan, M. Yao, J. Zhang, B. Li, C. Xing, X. Song, P. Su and H. Zhang, *Front. Chem.*, **8**, 261 (2020).
34. S. Zhang, N. Sun, X. He, X. Lu and X. Zhang, *J. Phys. Chem. Ref. Data*, **35**, 1475 (2006).
35. Toxicological review of acetonitrile, U.S. Environmental Protection Agency Washington, DC (1999), https://iris.epa.gov/static/pdfs/0205tr.pdf (Last visited 20/04/2022).
36. A. Janes and E. Lust, *J. Electroanal. Chem.*, **588**, 285 (2006).
37. F. Mirjalili, L. Chuah and E. Salahi, *Sci. World J.*, **2014**, 1 (2014).
38. R. Xu, H. Huang, Z. Tian, J. Xie and C. Lei, *Polymers*, **12**, 117 (2020).
39. E. Wang, C.-H. Chiu and P.-H. Chou, *J. Power Sources*, **461**, 228148 (2020).
40. G. Vardar, A. E. S. Sleightholme, J. Naruse, H. Hiramatsu, D. J. Siegel and C. W. Monroe, *ACS Appl. Mater. Interfaces*, **6**(20), 18033 (2014).
41. S. Shiraishi, *Carbon Alloy*, 447 (2003).
42. J. Lee, P. Srimuk, S. Fleischmann, X. Su, T. A. Hatton and V. Presser, *Progress Mater. Sci.*, **101**, 46 (2019).
43. E. R. Fadel, F. Faglioni, G. Samsonidze, N. Molinari, B. V. Merinov, W. A. Goddard III, J. C. Grossman, J. P. Mailoa and B. Kozinsky, *Nat. Commun.*, **10**, 3360 (2019).
44. J. Kalhoff, G. G. Eshetu, D. Bresser and S. Passerini, *ChemSusChem*, **8**(13), 2154 (2015).
45. S. Sopčić, D. Antonić and Z. Mandić, *J. Solid State Electrochem.*, **26**, 591 (2022).
46. R. Chen, D. Bresser, M. Saraf, P. Gerlach, A. Balducci, S. Kunz and S. Passerini, *ChemSusChem*, **13**(9), 2205 (2021).